Received: 12 February 2019 | Revised: 26 April 2019 | Accepted: 23 May 2019

DOI: 10.1002/mrm.27860

FULL PAPER

Magnetic Resonance in Medicine

Investigation of the influence of B_0 drift on the performance of the PLANET method and an algorithm for drift correction

Yulia Shcherbakova[1] | **Cornelis A.T. van den Berg**[2] | **Chrit T.W. Moonen**[1] | **Lambertus W. Bartels**[1]

[1]Center for Image Sciences, Imaging Division, University Medical Center Utrecht, Utrecht, Netherlands

[2]Department of Radiotherapy, Imaging Division, University Medical Center Utrecht, Utrecht, Netherlands

Correspondence
Yulia Shcherbakova, Center for Image Sciences, Imaging Division, University Medical Center Utrecht, Heidelberglaan 100, Room Q.03.4.21, 3508 GA Utrecht, Netherlands.
Email: Y.Shcherbakova@umcutrecht.nl

Funding information
The Netherlands Organisation for Scientific Research (NWO), Domain Applied and Engineering Sciences, Grant/Award Number: 12813

Purpose: The PLANET method was designed to simultaneously reconstruct maps of T_1 and T_2, the off-resonance, the RF phase, and the banding free signal magnitude. The method requires a stationary B_0 field over the course of a phase-cycled balanced SSFP acquisition. In this work we investigated the influence of B_0 drift on the performance of the PLANET method for single-component and two-component signal models, and we propose a strategy for drift correction.

Methods: The complex phase-cycled balanced SSFP signal was modeled with and without frequency drift. The behavior of the signal influenced by drift was mathematically interpreted as a sum of drift-dependent displacement of the data points along an ellipse and drift-dependent rotation around the origin. The influence of drift on parameter estimates was investigated experimentally on a phantom and on the brain of healthy volunteers and was verified by numerical simulations. A drift correction algorithm was proposed and tested on a phantom and in vivo.

Results: Drift can be assumed to be linear over the typical duration of a PLANET acquisition. In a phantom (a single-component signal model), drift induced errors of 4% and 8% in the estimated T_1 and T_2 values. In the brain, where multiple components are present, drift only had a minor effect. For both single-component and two-component signal models, drift-induced errors were successfully corrected by applying the proposed drift correction algorithm.

Conclusion: We have demonstrated theoretically and experimentally the sensitivity of the PLANET method to B_0 drift and have proposed a drift correction method.

KEYWORDS
B_0 drift, PLANET, quantitative MRI, relaxometry

1 | INTRODUCTION

Quantitative MRI is used widely to obtain quantitative characteristics of tissues related to their biological and physiological properties, based on which tissues can be differentiated and associated with specific diseases. The measurement of the relaxation times of tissues (or quantitative relaxometry) is particularly important for clinical applications in oncology and regenerative medicine.[1] Many different techniques exist for quantitative relaxometry, such as standard inversion recovery and multiecho spin-echo-based approaches,[2-4] many rapid SSFP approaches like inversion-recovery TrueFISP,[5,6] the variable flip angle approach or DESPOT-1 and DESPOT-2,[7-9] the triple-echo steady-state approach,[10] the MR fingerprinting approach,[11] and many others.

We recently introduced a method called PLANET to simultaneously reconstruct maps of the relaxation times T_1 and T_2, the local off-resonance Δf_0, the RF phase, and the banding free signal magnitude, using phase-cycled balanced SSFP (bSSFP) data.[12] The method is based on linear least-squares fitting of an ellipse to phase-cycled bSSFP data in the complex signal plane and subsequent analytical parameter estimation from the fitting results.

A bSSFP signal is strongly dependent on local resonant frequency, and the use of RF phase cycling shifts the off-resonance profile of the signal dependent on the RF phase increment. The main requirement of the PLANET model is a stationary main magnetic field (B_0) over the course of the acquisition, which usually consists of 8-10 dynamics and takes around 10 minutes for full brain coverage with FOV of 220 × 220 × 100 mm^3 and voxel size of 1 × 1 × 4 mm^3 (without any acceleration technique). In this case, accurate and precise parameter estimation can be achieved for a single-component voxel, as we showed in a previous study,[13] whereas systematic errors in parameter estimates are expected when multiple signal components with different relaxation times and frequencies are present within a voxel.[13]

Due to intensive gradient activity, the requirement of a stationary B_0 field can be difficult to meet, and as a result, B_0 drift can occur, which might result in errors in the estimated parameters. The severity of drift effect depends on the field strength, history of gradient activity and heating of metallic components of the scanner, the acquisition time, the used gradient mode, shimming, and more, which vary among different systems and over time.

The purpose of this work was to investigate the effects of B_0 drift and to assess the influence of drift on the quantitative parameters estimated using the PLANET method. We first derived a geometrical interpretation of the influence of drift on a single-component phase-cycled bSSFP signal based on a mathematical model. Subsequently, based on this geometrical interpretation, we developed a strategy for drift correction. Next, we experimentally showed the influence of drift on the parameter estimates for a single-component model in a phantom and for a 2-component model of white matter (WM) in the human brain. We assessed the effects of drift for both single-component and two-component signal models and evaluated the performance of the drift correction algorithm in both cases by looking at drift-induced errors in the quantitative parameter estimates. Finally, we performed numerical simulations for both single-component and two-component signal models to verify the experimental results.

2 | METHODS

2.1 | How drift influences a single-component phase-cycled bSSFP signal

For a single-component model with monoexponential transverse and longitudinal relaxation, the complex phase-cycled bSSFP signal can be represented as an ellipse in the complex plane[14,15] as follows:

$$I = M_{\text{eff}} \frac{1 - a e^{i(\theta_0 - \Delta\theta)}}{1 - b\cos\left(\theta_0 - \Delta\theta\right)} e^{i\varphi}, \tag{1}$$

where M_{eff}, a, and b are parametric functions of T_1, T_2, TR, and flip angle (FA); $\Delta\theta$ is the user-controlled RF phase increment (rad); $\varphi = 2\pi\left(\delta_{CS} + \Delta f_0\right) TE + \varphi_{RF}$ is the rotation angle of the ellipse around the origin with respect to its vertical form[14]; $\theta_0 = 2\pi\left(\delta_{CS} + \Delta f_0\right) TR$; Δf_0 is the local off-resonance (Hz); φ_{RF} is the combined RF transmit and receive phase; and δ_{CS} is the chemical shift of the species (Hz) with respect to the water peak.

After substitution, Equation 1 can be rewritten as

$$I = M_{\text{eff}} \frac{1 - a e^{i(2\pi(\delta_{CS} + \Delta f_0)TR - \Delta\theta)}}{1 - b\cos\left(2\pi\left(\delta_{CS} + \Delta f_0\right) TR - \Delta\theta\right)} e^{i(2\pi(\delta_{CS} + \Delta f_0)TE + \varphi_{RF})}. \tag{2}$$

A graphical representation of the ellipse described by this equation in the complex plane is shown in Figure 1A.

The frequency drift is modeled as $\Delta f_0 \rightarrow \Delta f_0 + \Delta f_{\text{drift}}(t)$, where $\Delta f_{\text{drift}}(t)$ is the time-dependent frequency drift during PLANET acquisition and is equal to $\gamma \Delta B_0(t)$, where γ is the gyromagnetic ratio equal to 42.58 MHz/T. Then Equation 2 becomes

$$I = M_{\text{eff}} \frac{1 - a e^{i\left(2\pi\left(\delta_{CS} + \Delta f_0\right)TR - \Delta\theta + 2\pi TR\Delta f_{\text{drift}}(t)\right)}}{1 - b\cos\left(2\pi\left(\delta_{CS} + \Delta f_0\right) TR - \Delta\theta + 2\pi TR\,\Delta f_{\text{drift}}(t)\right)} e^{i(2\pi(\delta_{CS} + \Delta f_0)TE + \varphi_{RF})} e^{i2\pi TE\,\Delta f_{\text{drift}}(t)} \tag{3}$$

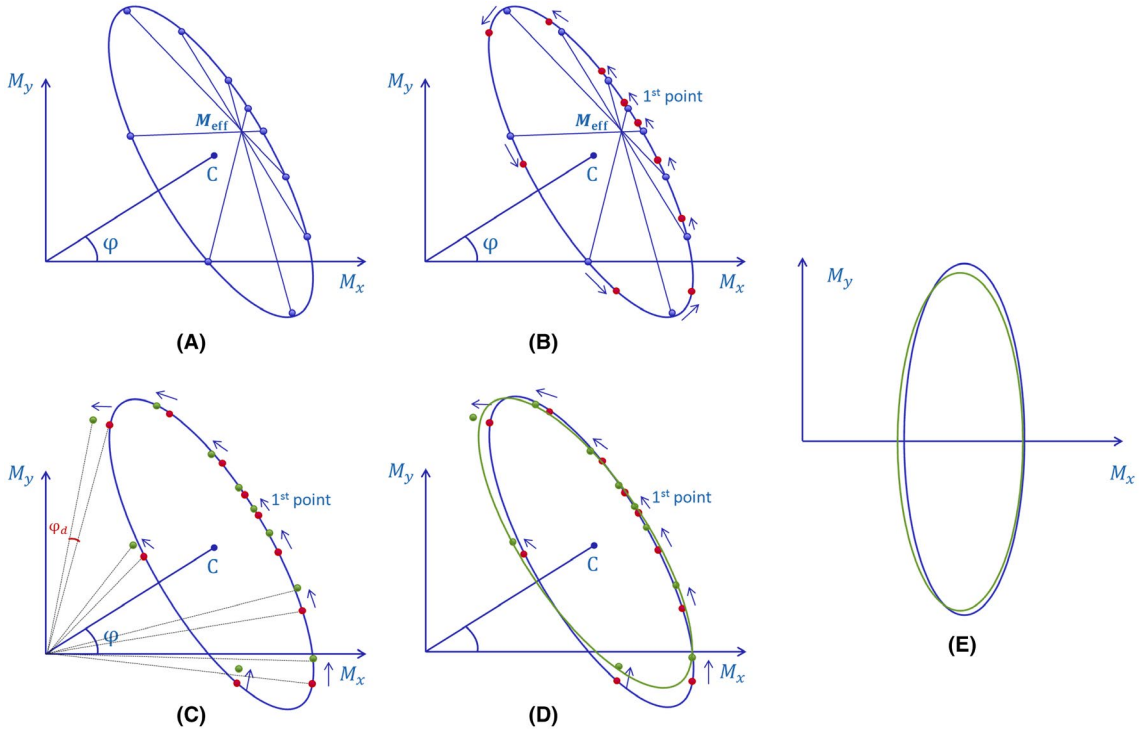

FIGURE 1 Schematic representation of the influence of B_0 drift on the data points in the complex signal plane. A, The ellipse without drift. B, Time-dependent displacement of the data points along the ellipse due to B_0 drift. The nondrifted data points (not influenced by drift) are blue; the displaced data points are red. C, Time-dependent rotation of the data points around the origin. The rotated data points are green. D, The ellipse without drift is blue, and the ellipse fitted to the drifted data points (influenced by drift) is green. E, The vertical conic forms of the ellipse without drift is blue, and the ellipse fitted to the drifted data points is green

The first part of Equation 3 multiplied by the first exponential represents the elliptical equation in Equation 2, but with a modified time-dependent RF phase-increment scheme: $\Delta\theta_{new}(t) = \Delta\theta - 2\pi TR\,\Delta f_{drift}(t)$. This corresponds to a drift-dependent displacement of all data points along the ellipse as illustrated in Figure 1B. Note that if only this effect of drift is taken into account, the data points remain on the "nondrifted" ellipse (i.e., the ellipse fitted to the data points not influenced by drift).

There is, however, another effect of the drift, caused by the last exponential factor in Equation 3. Using this factor, drift leads to an additional rotation of the data points around the origin, as illustrated in Figure 1C,D. As drift is time-dependent, the rotation angle differs per data point.

These 2 effects together relocate the data points in the complex plane away from the nondrifted ellipse and result in a nonelliptical distribution of the points. Ignoring the effects of B_0 drift, fitting an ellipse to the drifted data points (i.e., data points relocated by drift from their nondrifted positions) would lead to different fit results compared with the fit for the nondrifted case (Figure 1E). After performing PLANET postprocessing,[12] this would result in errors in the parameter estimates.

We propose a drift correction method that aims to relocate each data point back to the position in the complex plane that it would have in the case without drift.

2.2 | Drift correction method

Based on this analysis, we propose a 3-step drift correction algorithm:

1. Calculation of the spatio-temporal B_0 drift during the phase-cycled PLANET acquisition $\Delta f_{drift,n}(i, j)(t)$, where n is the number of the dynamic acquisition, t is the time, and (i, j) are the spatial indices of the voxel. One phase-cycled PLANET acquisition consists of N acquisitions. Assuming temporally linear drift over the duration of the phase-cycled PLANET acquisition, the frequency drift over the nth phase-cycled acquisition is estimated by

$$\Delta f_{drift,n}(i,j)(t) = n * \frac{\Delta f_{total\ drift}(i,j)}{N}(Hz), n = \{1, \ldots N\}, \quad (4)$$

where the total drift over the phase-cycled PLANET acquisition $\Delta f_{total\ drift}(i, j)$ is calculated by subtracting

2 reference B_0 maps acquired right before and right after PLANET acquisition, and $t = n\Delta t$ is the time point within the PLANET acquisition scheme corresponding to nth dynamic acquisition, where the dynamic acquisitions in the phase-cycled acquisition each have a duration Δt.

2. Correction of M_{eff}, T_1, and T_2 by multiplying the experimental complex data by $e^{-i2\pi TE\,\Delta f_{\text{drift},n}(i,j)(t)}$, the geometrical equivalent of which is the rotation of each drifted data point around the origin back to the nondrifted ellipse.
3. Correction of Δf_0 and φ_{RF} by defining $\Delta\theta_{\text{new}}(i,j)(t) = \Delta\theta_n - 2\pi TR\,\Delta f_{\text{drift},n}(i,j)(t)$, which geometrically moves the drifted data points along the ellipse back to their nondrifted positions, where $\Delta\theta_n$ is the user-controlled RF phase increment $\Delta\theta_n = (n-1) * \frac{2\pi}{N} - \pi$, $n = \{1, 2 \ldots N\}$, covering a full cycle of 2π.

2.3 | Temporal drift model

As we observed experimentally, B_0 drift on a long-time scale can be represented by an exponential function. In the proposed drift correction algorithm, we assumed the temporal evolution of the drift to be linear over the duration of 1 PLANET acquisition.

Here we compared 2 temporal drift models:

- A linear model described by Equation 4; and
- An exponential model described by

$$\Delta f_{\text{drift},n}(i,j)(t) = A_{\text{drift}}(i,j)\left(1 - exp\left(-\frac{t}{b_{\text{drift}}(i,j)}\right)\right), \quad (5)$$

where $\Delta f_{\text{drift},n}(i,j)(t)$ is the frequency drift over time t, A_{drift} and b_{drift} are parameters describing the global spatial drift characteristics, and (i, j) are the spatial indices of the voxel.

2.4 | Accuracy and precision in the estimated parameters and drift correction performance

The accuracy of the method was assessed by calculating relative errors (ε) in T_1, T_2, Δf_0, and φ_{RF} estimates before and after drift correction, as follows:

$$\varepsilon_X = \frac{\bar{X} - X_{true}}{X_{true}} \cdot 100\%, \varepsilon_{X_{cor}} = \frac{\overline{X_{cor}} - X_{true}}{X_{true}} \cdot 100\%. \quad (6)$$

The precision of the method was assessed by calculating the relative SD of T_1, T_2, Δf_0, and φ_{RF} estimates before and after drift correction, as follows:

$$SD_X = \frac{\sqrt{\frac{1}{Z}\sum_{i=1}^{Z}\left(X^i - \bar{X}\right)^2}}{\bar{X}} \cdot 100\%,$$
$$SD_{X_{cor}} = \frac{\sqrt{\frac{1}{Z}\sum_{i=1}^{Z}\left(X^i_{cor} - \overline{X_{cor}}\right)^2}}{\overline{X_{cor}}} \cdot 100\%, \quad (7)$$

where $\bar{X} = \frac{1}{Z}\sum_{i=1}^{Z} X^i$ refers to the average of the values X^i affected by drift; $\overline{X_{cor}} = \frac{1}{Z}\sum_{i=1}^{Z} X^i_{cor}$ refers to the average of the values X^i_{cor} estimated after drift correction, assuming a true value of X_{true} for parameters T_1, T_2, Δf_0, and φ_{RF}; i is an index for the voxels in a region of interest (ROI) (in experiments) or the current number of the simulation (in numerical simulations); and Z is the total number of voxels in an ROI (in experiments) or the total number of simulations (in numerical simulations).

To quantify the drift correction on T_1, T_2, Δf_0, and φ_{RF} estimates, Δ_{cor} were determined as

$$\Delta_{corT_1} = T_{1cor} - T_{1uncor}, \quad \Delta_{corT_2} = T_{2cor} - T_{2uncor},$$
$$\Delta_{cor\,\Delta f_0} = \Delta f_{0cor} - \Delta f_{0uncor}, \quad \Delta_{cor\varphi_{RF}} = \varphi_{RF_{cor}} - \varphi_{RF_{uncor}}, \quad (8)$$
$$\Delta_{corT_1}(\%) = \frac{T_{1cor} - T_{1uncor}}{T_{1cor}} \cdot 100\%, \quad \Delta_{corT_2}(\%) = \frac{T_{2cor} - T_{2uncor}}{T_{2cor}} \cdot 100\%.$$

2.5 | Experiments

2.5.1 | Phantom experiments

To investigate the effects of drift on a single-component phase-cycled bSSFP signal model, and to test the drift correction algorithm, MRI experiments on a phantom (1.5-L plastic bottle filled with an aqueous solution of $MnCl_2{\cdot}4H_2O$ [concentration of approximately 55-60 mg/L]) were performed on a clinical 1.5T MR scanner (Ingenia; Philips, Best, Netherlands). A 15-channel head coil was used as a receiver. The experimental design is shown in Figure 2A.

To compare two temporal drift models, after the first reference B_0 mapping acquisition we repeated 5 times the PLANET acquisition over the course of a 65-minute experiment. Each PLANET acquisition was followed by the reference B_0 mapping acquisition. This allowed us to assess the performance of the linear drift correction method in the presence of more pronounced long-term drift, which is expected to be nonlinear. Six reference B_0 maps were acquired over the course of a 65-minute experiment, alternated with phase-cycled PLANET acquisitions. The reference B_0 maps were obtained using a dual-echo approach. The B_0 drift over the duration of each PLANET acquisition was calculated by subtracting the two reference B_0 maps acquired just before and after the PLANET acquisition concerned.

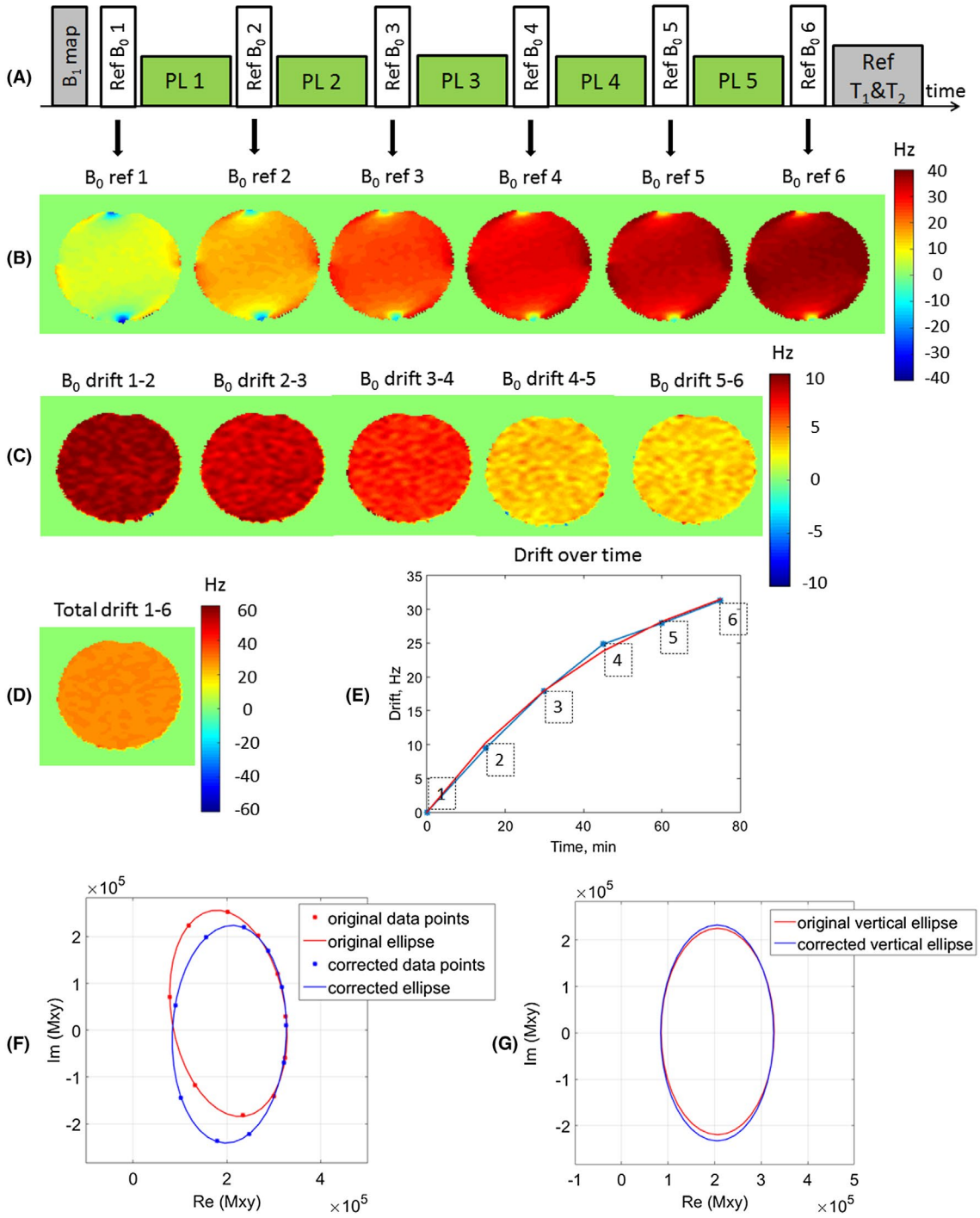

FIGURE 2 Experimental drift measurements in the phantom. A, Experimental design. B, Reference B_0 maps (obtained in 3D and shown only for 1 axial slice of the phantom). C, Calculated B_0 drift maps. D, Total drift map. E, Drift over 65-minute interval for 1 voxel in the center of the slice: Exponential temporal drift curve (red) fitted to the experimental data points (blue dots); lines connecting the experimental data points (blue). F, The example of original (measured) data points and drift-corrected data points with corresponding elliptical fits for 1 voxel in the middle of the slice. G, Example of original vertical ellipse and drift-corrected vertical ellipse for 1 voxel in the center of the slice

For the PLANET acquisition with more severe drift, the T_1, T_2, Δf_0, and φ_{RF} maps were reconstructed. Both linear and exponential temporal drift models were used to correct the drift over this PLANET acquisition; T_1, T_1, T_2, Δf_0, and φ_{RF} maps were recalculated by applying the drift correction. Because T_1 estimates depend on FA (see Equation 10 in Shcherbakova[12]), a B_1 mapping sequence was acquired, and voxel-wise B_1 correction was performed while calculating the T_1 maps. The B_1 maps were calculated using a dual-TR actual FA imaging technique.[16] The reference T_1 and T_2

TABLE 1 Protocol parameter settings

Phantom experiment at 1.5 T											
PLANET: 3D phase-cycled bSSFP											
FOV (m^3)	Voxel size (mm^3)	Acq. matrix	Rec. matrix	TR (ms)	TE (ms)	Flip angle	Number of RF increment steps	NSA	Readout direction	Dummy pulses	Total scan time (minutes)
160 × 160 × 159	1.1 × 1.1 × 3	144 × 145 × 53	160 × 160 × 53	10	5	30	10	1	AP	6 seconds for each dynamic	13:46
Reference B_1 map (3D dual-TR SPGR)											
FOV (m^3)	Voxel size (mm^3)	Acq. matrix	Rec. matrix	TR (ms)	TE (ms)	Flip angle	NSA	Readout direction	Parallel imaging	Total scan time (minutes)	
160 × 160 × 159	2.5 × 4 × 3	64 × 40 × 53	160 × 160 × 53	[30; 150]	1.82	60	1	AP	SENSE 2 in RL	03:12	
Reference off-resonance map (3D dual-echo SPGR)											
FOV (m^3)	Voxel size (mm^3)	Acq. matrix	Rec. matrix	TR (ms)	TE (ms)	Flip angle	NSA	Readout direction	Parallel imaging	Total scan time (minutes)	
160 × 160 × 159	2.5 × 4 × 3	64 × 40 × 53	160 × 160 × 53	30	[4.6; 9.2]	60	1	AP	SENSE 2 in RL	01:04	
Reference T_1 and T_2 map (2D MIXED)											
FOV (m^3)	Voxel size (mm^3)	Acq. matrix	Rec. matrix	TR SE (ms)	TR IR (ms)	IR delay (ms)	TE (ms)	NSA	Readout direction	Total scan time (minutes)	
160 × 160 × 3	2 × 2 × 3	80 × 80 × 1	160 × 160 × 1	1500	2000	500	[30; 60; 90; 120; 150; 180]	1	AP	04:47	
In vivo experiments at 1.5 T and 3 T											
PLANET: 3D phase-cycled bSSFP											
FOV (m^3)	Voxel size (mm^3)	Acq. matrix	Rec. matrix	TR (ms)	TE (ms)	Flip angle	Number of RF increment steps	NSA	Readout direction	Dummy pulses	Total scan time (minutes)
220 × 220 × 100	0.98 × 0.98 × 4	220 × 220 × 25	224 × 224 × 25	10	5	20	10	1	AP	10 seconds for each dynamic	11:00
Reference B_1 map (3D dual-TR SPGR)											
FOV (m^3)	Voxel size (mm^3)	Acq. matrix	Rec. matrix	TR (ms)	TE (ms)	Flip angle	NSA	Readout direction	Parallel imaging	Total scan time (minutes)	
220 × 220 × 100	3.44 × 4 × 4	64 × 55 × 25	224 × 224 × 25	[30; 150]	1.82	60	1	AP	SENSE 1.5 in RL	02:43	
Reference off-resonance map (3D dual-echo SPGR)											

(Continues)

TABLE 1 (Continued)

Phantom experiment at 1.5 T										
FOV (m^3)	Voxel size (mm^3)	Acq. matrix	Rec. matrix	TR (ms)	TE (ms)	Flip angle	NSA	Readout direction	Parallel imaging	Total scan time (minutes)
220 × 220 × 100	3.44 × 4 × 4	64 × 40 × 53	224 × 224 × 25	30	[4.6; 9.2]	60	1	AP	No	01:21
Reference T_1 and T_2 map (2D MIXED)										
FOV (m^3)	Voxel size (mm^3)	Acq. matrix	Rec. matrix	TR SE (ms)	TR IR (ms)	IR delay (ms)	TE (ms)	NSA	Readout direction	Total scan time (minutes)
220 × 220 × 4	2 × 2 × 4	80 × 80 × 1	112 × 110 × 1	2500	5000	500	[30; 60; 90; 120; 150; 180; 210; 240]	1	AP	14:00

Abbreviations: AP, anterior–posterior; bSSFP, balanced SSFP; IR, inversion recovery; NSA, number of signals averaged; RL, right–left; SE, spin echo; and SPGR, spoiled gradient echo.

values of the phantom were measured using a simultaneous spin-echo and inversion-recovery method (2D MIXED).[3] Relevant protocol parameter settings are presented in Table 1.

The accuracy and precision in the parameter estimates, before and after linear drift correction, were assessed using Equations 6 and 7. Deviations quantifying the drift correction performed on T_1, T_2, Δf_0, and φ_{RF} estimates were calculated using Equation 8. The ROI analysis was performed on the quantitative T_1 and T_2 maps calculated for the phantom: The ROI (approximately 2000 voxels) was placed in the center of the phantom on the selected slice.

2.5.2 | In vivo experiments

To investigate the effects of drift for a tissue in which multiple components are present, and to test the drift correction algorithm, experiments on the brain of healthy volunteers were performed on clinical 1.5T and 3T MR scanners. Both protocols included B_1 mapping acquisition, one PLANET acquisition in between two reference B_0 mapping acquisitions, and the reference T_1 and T_2 mapping acquisition with the protocol parameter settings given in Table 1.

A 2.5-ms-long RF excitation pulse was used in each PLANET acquisition to minimize magnetization transfer effects.[17] Image registration (rigid) and Gibbs ringing filtering[18] were applied to the brain data before performing the PLANET reconstruction. The B_0 drift maps were filtered (using a circular averaging filter with radius of 15) before applying the drift correction algorithm.

The T_1, T_2, Δf_0, and φ_{RF} maps were calculated before and after drift correction. The B_1 correction was performed voxel-wise while calculating the T_1 maps. Deviations quantifying the drift correction performed on T_1, T_2, Δf_0, and φ_{RF} estimates were calculated using Equation 8. The ROI analyses were performed on the quantitative T_1 and T_2 maps for both 1.5T and 3T data. The ROIs were manually delineated in WM on the selected slice in the area where the drift was the most pronounced (each ROI was approximately 100-150 voxels). The precision of the T_1 and T_2 measurements was evaluated by calculating SDs on T_1 and T_2 maps over the ROIs.

2.6 | Numerical simulations

2.6.1 | Drift-induced errors and drift correction for a single-component signal model

To investigate the errors caused by B_0 drift for a single-component tissue model, numerical simulations were performed with relaxation times equal to those of the phantom material: $T_1 = 430$ ms and $T_2 = 50$ ms. The following parameter settings were used in the simulations: FA in the range of 0°-45°, TR in the range of 0-20 ms, 10 RF phase-increment values $\Delta\theta_n = \frac{2\pi n}{10} - \pi$, $n = \{0, 1, .., 9\}$, $M_{eff} = 10\,000$, single peak with $\delta_{CS} = 0$, $\Delta f_0 = 5$ Hz,

and $\varphi_{RF} = -0.2$ rad (these values were obtained experimentally in the phantom). The B_0 drift was assumed to be linear over time and spatially independent (Δf_{drift} = [1 2 3 4 5 6 7 8 9 10] Hz), as we found in the experimental results in the phantom. Gaussian noise was added independently to the real and imaginary data, resulting in an SNR of about 230, which corresponds to the experimentally measured SNR in the phantom. The number of performed Monte Carlo simulations was 10 000.

The accuracy and precision in the T_1, T_2, Δf_0, and φ_{RF} estimates were assessed using Equations 6 and 7.

2.6.2 | Drift-induced errors and drift correction for a 2-component signal model

To investigate the errors in the parameter estimates caused by B_0 drift in the case in which two components are present in the signal, numerical simulations were performed for WM tissue at 3 T, which is known to be a two-component tissue.[19,20] Two single peaks were used in the simulations: the on-resonant dominant component and the smaller component with an average frequency shift of $\Delta f = 20$ Hz.[20] The dominant component has $T_{1D} = 1000$ ms and $T_{2D} = 80$ ms, with a volume fraction of 0.88; the smaller component has $T_{1S} = 400$ ms and $T_{2S} = 10$ ms, with a myelin water fraction of 0.12. The off-resonance $\Delta f_0 = 10$ Hz was used, and the RF phase offset $\varphi_{RF} = -0.15$ rad was used. Gaussian noise was added independently to the real and imaginary data, resulting in an SNR ranging from 30 to 150. The number of performed Monte Carlo simulations was 10 000.

The simulations were performed using the complex phase-cycled bSSFP signal described by Equations 7 and 8 in our previous study[13] for 3 cases:

- No B_0 drift;
- Linearly increasing over time and spatially independent frequency drift Δf_{drift} = [1 2 3 4 5 6 7 8 9 10] Hz; and
- Linearly increasing over time and spatially independent frequency drift Δf_{drift} = [1 2 3 4 5 6 7 8 9 10] Hz with subsequently applied proposed drift correction algorithm.

The accuracy and precision in the T_1, T_2, Δf_0, and φ_{RF} estimates were assessed using Equations 6 and 7, where the true parameter values were taken for the dominant WM component.

All simulations and calculations were performed in MATLAB R2015a (The MathWorks, Natick, MA).

3 | RESULTS

3.1 | Experimental results in the phantom

Experimental results in the phantom are shown in Figure 2. Six reference B_0 maps acquired before and after each of 5 PLANET acquisitions and the corresponding calculated B_0 drift maps are presented in Figure 2B,C. A total drift of 28 Hz over a 65-minute scanning session was observed (Figure 2D). The temporal drift was analyzed voxel-wise, and the example of the experimental data for 1 voxel (in the center of the phantom) is shown in Figure 2E. Over a 65-minute scanning time the temporal drift can be considered as an exponential function. Over the 11-minute duration of the PLANET acquisition, the drift with an average value of 10 Hz can be very well approximated with a linear function.

As an example, the initial data points and the data points after drift correction for 1 voxel are shown in Figure 2F, with corresponding elliptical fits. The conic vertical forms of these ellipses are shown in Figure 2G. The ellipses are different, as expected due to the drift.

The estimated T_1, T_2, Δf_0, and φ_{RF} maps of the phantom before and after linear drift correction, as well as the reference T_1, T_2, and Δf_0 maps, are shown in Figure 3A-C. The drift correction was performed for the first PLANET acquisition, where the drift was more severe. The performance of linear and exponential drift correction was very similar; therefore, we did not include the maps of T_1, T_2, Δf_0, and φ_{RF} after exponential drift correction in Figure 3. A reference RF phase map was not acquired and therefore is not shown. Deviations quantifying the amount of linear drift correction performed on all quantitative parameters are shown in Figure 3D,E. The drift correction decreased the T_1 values by about 4%, increased the T_2 values by about 8%, decreased the Δf_0 values by about 120%, and increased the φ_{RF} values by about 3%. The magnitude image with white vertical and horizontal lines used for T_1 and T_2 profiles, and T_1 and T_2 profiles on estimated, corrected, and reference maps, are shown in Figure 3F,G. The T_2 estimates are more sensitive to the drift than T_1 estimates.

The quantitative ROI analysis for parameters T_1, T_2, Δf_0, and the relative errors in these parameters before and after drift correction, are presented in Supporting Information Table S1. The T_1 values were overestimated due to drift by around 5% compared with the reference values, and the corrected T_1 values were in agreement with the reference values with an accuracy of 1%. The T_2 values were underestimated due to drift by about 10% compared with the reference values, and after drift correction they were in agreement with the reference values with an accuracy of 2%. The Δf_0 values estimated by means of PLANET were about 80% overestimated due to drift, and after drift correction they became similar to the reference Δf_0 acquired right before PLANET acquisition.

Despite the fact that there are no directly visible B_0 drift-related artifacts in quantitative parameter maps, there are B_0 drift-related errors in the quantitative T_1, T_2, and Δf_0 maps.

3.2 | Experimental results in the brain

3.2.1 | 1.5 T

The results of the experiment in the brain of a healthy volunteer at 1.5 T are shown in Figure 4. The results are presented for 1 central slice. Spatially homogeneous drift was observed

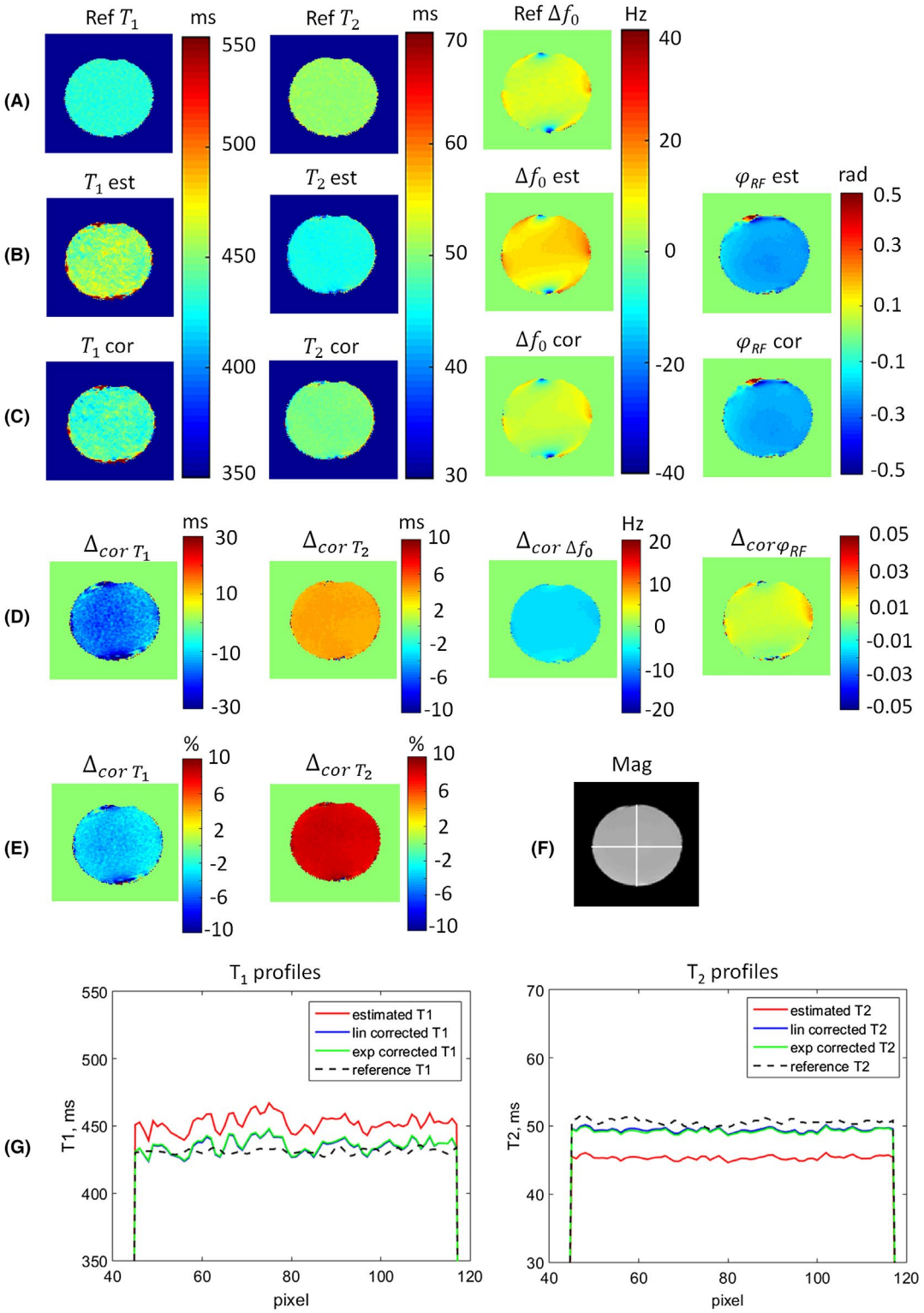

FIGURE 3 Experimental results in the phantom. A, Reference T_1, T_2, and Δf_0 maps. B, The T_1, T_2, Δf_0, and φ_{RF} maps before drift correction. C, The T_1, T_2, Δf_0, and φ_{RF} maps after linear drift correction. D, Maps of absolute Δ_{cor} quantifying the drift correction performed on T_1, T_2, Δf_0, and φ_{RF}. E, Maps of relative Δ_{cor} quantifying the drift correction performed on T_1 and T_2. F, Magnitude image with white vertical and horizontal lines in the center of the slice, used for T_1 and T_2 profiles. G, The T_1 and T_2 profiles (T_1 and T_2 values representing single voxels along the selected lines on estimated, corrected, and reference maps). The values were averaged voxel-wise between the horizontal and vertical selected lines

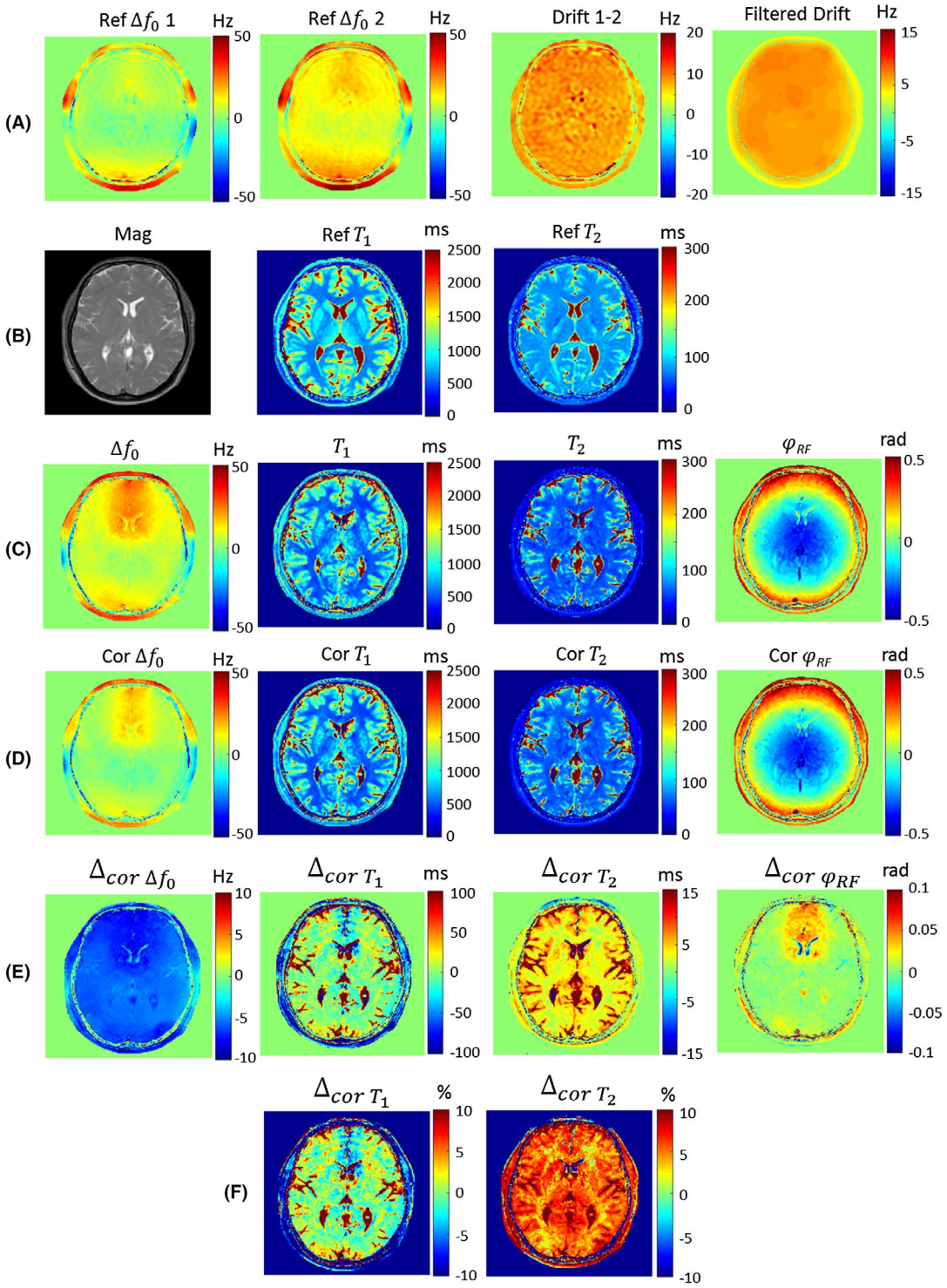

FIGURE 4 Experimental results obtained in the brain at 1.5 T. A, Reference B_0 maps before (1) and after (2) PLANET acquisition, the corresponding drift map (1,2), and the drift map filtered using a circular averaging filter. B, Banding-free magnitude image, the reference T_1 and T_2 maps. C, The T_1, T_2, Δf_0, and φ_{RF} maps before drift correction. D, The T_1, T_2, Δf_0, and φ_{RF} maps after linear drift correction. E, Maps of absolute Δ_{cor} quantifying the drift correction performed on Δf_0, T_1, T_2, and φ_{RF}. F, Maps of relative Δ_{cor} quantifying the drift correction performed on T_1 and T_2

over 11-minute PLANET acquisition (Figure 4A) with an average value of 9 Hz. The T_1, T_2, Δf_0, and φ_{RF} maps before and after linear drift correction are shown in Figure 4C,D. The banding-free magnitude and the reference T_1 and T_2 maps are shown in Figure 4B. Deviations quantifying the amount of linear drift correction performed on all parameters are shown in Figure 4E. The mean T_1 and T_2 values were calculated for WM. The results of the ROI analysis are given

TABLE 2 Quantitative results from the experiments in the brain at 1.5 T and 3 T: estimated, drift-corrected, and reference T_1 and T_2 values in white matter

1.5 T	Estimated values		Drift-corrected values		Reference values		Literature-published values[a]	
ROI	T_1	T_2	T_1	T_2	T_1	T_2	T_1	T_2
1	508 ± 34	55 ± 3	501 ± 26	61 ± 2	596 ± 21	76 ± 2	621 ± 61 (9)	58 ± 4 (9)
2	460 ± 33	55 ± 3	458 ± 20	57 ± 3	596 ± 19	77 ± 3	561 ± 12 (21)	73 ± 2 (21)
3	475 ± 30	56 ± 4	475 ± 32	58 ± 4	595 ± 27	84 ± 4		
4	495 ± 33	57 ± 5	487 ± 38	58 ± 5	629 ± 24	85 ± 5		
Mean	485 ± 33	56 ± 4	480 ± 30	59 ± 4	604 ± 23	81 ± 4		

3T	Estimated values		Drift-corrected values		Reference values		Literature-published values	
ROI	T_1	T_2	T_1	T_2	T_1	T_2	T_1	T_2
1	678 ± 33	51 ± 2	664 ± 35	53 ± 2	771 ± 19	68 ± 2	832 ± 1 (22)	80 ± 1 (22)
2	660 ± 42	50 ± 3	642 ± 39	53 ± 3	781 ± 18	70 ± 3	1084 ± 45 (23)	69 ± 3 (23)
3	636 ± 30	50 ± 2	624 ± 29	53 ± 2	771 ± 16	69 ± 2	781 ± 61 (24)	65 ± 6 (24)
Mean	658 ± 36	50 ± 2	643 ± 35	53 ± 2	774 ± 18	69 ± 2		

Note: The mean T_1 and T_2 values at 1.5 T were calculated for 1 slice of the brain by averaging over 4 regions of interest (ROIs) (each around 150 voxels) in white matter on corresponding T_1 and T_2 maps. The mean T_1 and T_2 values at 3 T were calculated for 1 slice of the brain by averaging over 3 ROIs (each around 100 voxels) in white matter on corresponding T_1 and T_2 maps.
[a]Numbers in parentheses are reference citations.

in Table 2 for the estimated, drift-corrected, reference, and literature-published T_1 and T_2 values.

After drift correction, T_1 values decreased by about 1% compared with the uncorrected values, and T_2 values increased by about 5% compared with the uncorrected values (Figure 4E,F and Table 2). The B_0 values decreased by about 50%, and the corrected B_0 map resembles the reference B_0 map acquired right before the PLANET acquisition. The RF phase maps almost did not change after drift correction.

3.2.2 | 3 T

A spatially inhomogeneous drift was observed over the same 11-minute PLANET acquisition in the brain of another healthy volunteer at 3 T, with a maximum value of 10 Hz for the selected slice (Figure 5A). The T_1, T_2, Δf_0, and φ_{RF} maps before and after linear drift correction, the banding-free magnitude, and the reference T_1 and T_2 maps, and deviations quantifying the amount of linear drift correction performed on all parameters are shown. The results of the ROI analysis are given in Table 2. Similar to the results at 1.5 T, the T_1 values after drift correction did not change much; they locally decreased by about 2% compared with the uncorrected values in the area with more pronounced drift. The T_2 values were more sensitive to drift, and after drift correction they increased by about 5%-6% compared with the uncorrected values in the area with more pronounced drift (Figure 5E,F and Table 2). The B_0 values decreased by about 50%, and the corrected B_0 map resembles the reference B_0 map acquired just before the PLANET acquisition. The RF phase maps did not change much after drift correction.

A remaining underestimation of about 20% in T_1 values and about 30% in T_2 values compared with the reference values are found in Figures 4 and 5 and Table 2.

3.3 | Simulation results

3.3.1 | Single-component phase-cycled bSSFP signal model of the phantom

Relative errors and SDs in T_1, T_2, Δf_0, and φ_{RF} estimates for a single-component signal model of the phantom are presented in Figure 6, affected by linear drift (Figure 6A,B) and after applying drift correction (Figure 6C,D). As shown, drift induced errors depend on the choice of FA and TR. For the combination of FA = 30° and TR = 10 ms, which was used in the experimental setup, the quantitative analysis of the errors is presented in Table 3. The T_1 values are overestimated due to drift by about 4% compared with the true values; T_2 values are underestimated due to drift by about 8% compared with the true values; Δf_0 values are overestimated due to drift by about 100%; and φ_{RF} values are underestimated due to drift by about 5%. After applying the proposed drift-correction algorithm, relative errors in all estimated

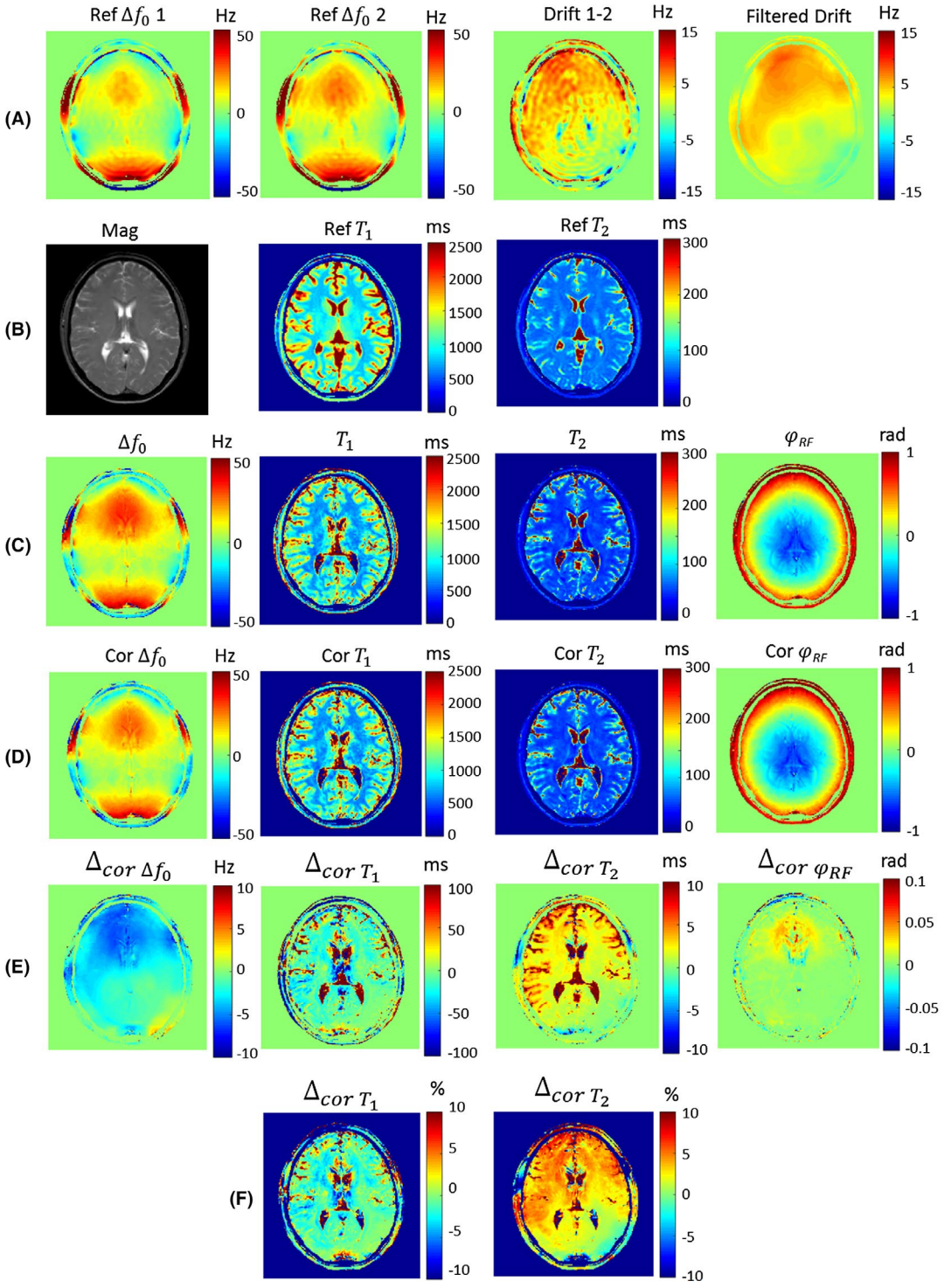

FIGURE 5 Experimental results obtained in the brain at 3 T. A, Reference B_0 maps before (1) and after (2) PLANET acquisition, the corresponding drift map (1,2), and drift map filtered using a circular averaging filter. B, Banding-free magnitude image, the reference T_1 and T_2 maps. C, The T_1, T_2, Δf_0, and φ_{RF} maps before drift correction. D, The T_1, T_2, Δf_0, and φ_{RF} maps after linear drift correction. E, Maps of absolute Δ_{cor} quantifying the drift correction performed on Δf_0, T_1, T_2, and φ_{RF}. F, Maps of relative Δ_{cor} quantifying the drift correction performed on T_1 and T_2

parameters are almost zero, which demonstrates an accurate performance of drift correction. The SDs in all estimated parameters are not affected by drift correction much and are below 5%.

These results are in agreement with the experimental results for the phantom shown previously: The simulated expected errors due to drift match the calculated errors in the estimated parameters.

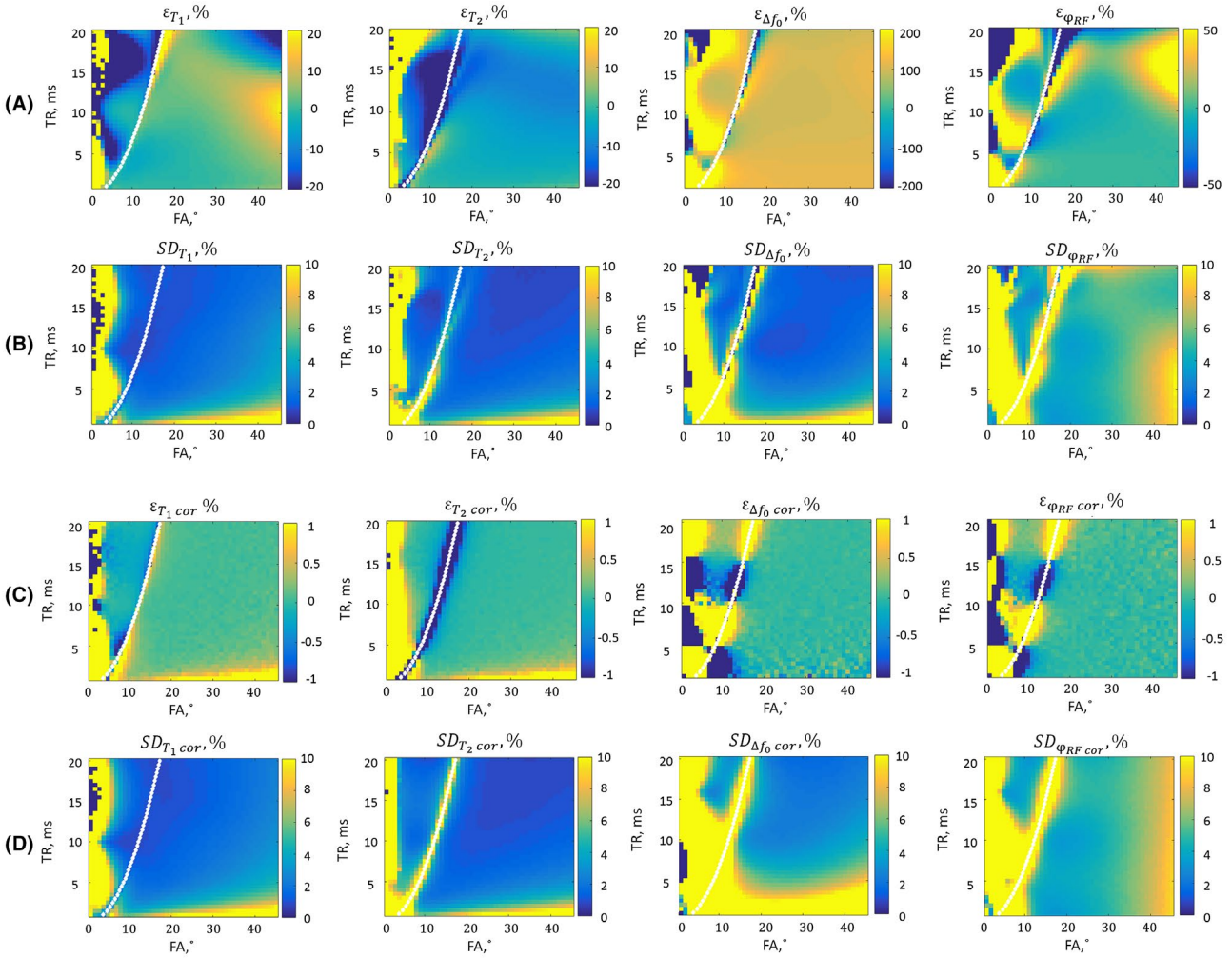

FIGURE 6 Simulation results for a single-component signal model. A,B, Relative errors (ε) and relative SDs in T_1, T_2, Δf_0, and φ_{RF} estimates (in percent) compared with their true values in the presence of linear over time and spatially independent drift: Δf_{drift} = [1 2 3 4 5 6 7 8 9 10] Hz. C,D, Relative errors (ε) and relative SDs in T_1, T_2, Δf_0, and φ_{RF} estimates (in percent) compared with their true values after applying linear drift-correction algorithm. The initial settings: T_1 = 430 ms, T_2 = 50 ms, Δf_0 = 5 Hz, φ_{RF} = −0.2 rad, and 10 RF phase increments

3.3.2 | Two-component phase-cycled bSSFP signal model

The simulation results for a two-component signal model of WM are shown in Figure 7. Relative errors in T_1, T_2, Δf_0, and φ_{RF} are shown for 3 cases: no drift, linear drift, and after applying the drift-correction algorithm. The errors in the estimated parameters depend on the choice of FA and TR. As we showed in a previous study,[13] in WM brain tissue the PLANET postprocessing results in systematic errors in estimated T_1, T_2, and Δf_0 values due to the presence of a second myelin-related component in WM. Here we can observe similar behavior for the case without drift.

For the combination of FA = 20° and TR = 10 ms, which was used in the experimental setup, the quantitative analysis of the errors is presented in Table 3. The T_1 values are underestimated by 30% without drift, underestimated by 29.5% in the presence of drift, and underestimated by 30.5% after drift correction. The T_2 values are underestimated by 35% without drift, underestimated by 39% in the presence of drift, and underestimated by 34.5% after drift correction. The Δf_0 values are overestimated by 14% without drift, overestimated by 58% in the presence of drift, and overestimated by 10% after drift correction. The φ_{RF} values are overestimated by 20% without drift, overestimated by 25% in the presence of drift, and overestimated by 23% after drift correction.

The drift correction performed on all estimated parameters predicted by the simulations for the combination of TR = 10 ms and FA = 20° is similar to the drift correction performed experimentally in the brain: After drift correction, T_1 values decreased by about 1% compared with the drift-corrected values; T_2 values increased by about 5% compared with the drift-corrected values; Δf_0 values decreased by about 48%; and φ_{RF} values decreased slightly by about 1.5%. In all cases, drift-induced errors were corrected.

TABLE 3 Quantitative results of simulations for a single-component signal model of the phantom and a two-component signal model of WM at 3 T: the accuracy and precision in T_1, T_2, Δf_0, and φ_{RF} estimates without drift, with drift, and after drift correction

	Single-component model of the phantom, TR = 10 ms, FA = 30°		Two-component signal model of WM at 3 T, TR = 10 ms, FA = 20°	
Parameter	Relative error ε, %	SD, %	Relative error ε, %	SD, %
No drift				
T_1	0.07	1.7	−30.2	2.1
T_2	0.04	1.0	−34.8	1.4
Δf_0	−0.01	2.8	13.7	1.5
φ_{RF}	−0.01	4.7	20.0	5.6
Drift				
T_1	4.2	1.9	−29.5	2.0
T_2	−7.5	1.1	−38.8	1.5
Δf_0	97.8	1.2	58.3	1.4
φ_{RF}	−4.7	4.8	24.7	6.9
Drift-corrected				
T_1	0.06	1.8	−30.6	1.9
T_2	0.03	1.1	−34.3	1.5
Δf_0	0.01	2.7	10.1	1.9
φ_{RF}	0.01	4.5	23.2	6.7

FA, flip angle; and WM, white matter.

4 | DISCUSSION

The PLANET method requires a stationary main magnetic field over the course of the acquisition. This requirement, however, can be difficult to meet, and as a consequence, B_0 drift can occur. In this work, we investigated the sensitivity of the PLANET method to B_0 drift and assessed the errors that drift can cause in the estimated T_1, T_2, Δf_0, and φ_{RF} parameters.

We presented a mathematical interpretation of the influence of drift on the elliptical phase-cycled bSSFP single-component signal behavior and proposed a general strategy for drift correction. We demonstrated how drift influences the performance of the PLANET method experimentally in a phantom and in the brain of healthy volunteers. Consequently, we verified the effects of the drift by performing numerical simulations for the same phantom and in vivo setups.

The experimental results in the phantom showed that the drift of about 10 Hz, which occurred over the 11-minute duration of the PLANET acquisition, induced the errors in estimated quantitative parameters: The T_1 values were overestimated due to drift by about 5%; the T_2 values were underestimated due to drift by about 10%; and the Δf_0 values were overestimated due to drift by about 80% compared with the corresponding reference values. The variance in the estimated parameters only slightly changed after drift correction. We demonstrated that both linear and exponential correction algorithms performed identically. The linear model for temporal evolution of the drift on a short time scale (0-15 minutes) may be a fair approximation of the exponential drift in the experiments reported in this paper. Drift-induced errors in T_1, T_2, Δf_0, and φ_{RF} estimates in a phantom were successfully corrected by applying the drift-correction algorithm. These results obtained experimentally were verified by numerical simulations for a similar setup: The bias and variance in all parameter estimates predicted by simulations matched the ones calculated using the experimental data of the phantom.

The investigation of the drift effects in the human brain showed that similar drift of about 10 Hz over the 11-minute duration of the PLANET acquisition had a significant effect only on the estimated Δf_0 values: An overestimation of about 50% in Δf_0 values was caused by drift. The other quantitative parameters were only affected slightly: The drift induced an overestimation of about 1% in T_1 estimates, an underestimation of about 5% in T_2 estimates, and an overestimation of about 5% in φ_{RF} estimates. The errors in the quantitative parameters calculated in the brain were in agreement with errors predicted by simulations for a similar experimental setup. The proposed drift-correction algorithm performed well and corrected the errors caused by drift. However, the remaining underestimation by about 20%-30% in T_1 and T_2 values compared with the reference and literature published values, which can be found in Figures 4 and 5 and Table 2, is not caused by B_0 drift. It is caused by the effect that in WM tissue where multiple components are present, a single-component PLANET model is not valid, as we already pointed out in a previous study.[13] Obviously, such underlying errors were not and cannot be corrected by the drift-correction algorithm. Keep in mind that any other techniques that assume a single-component relaxation model will fail in this case as well.

The severity of drift effect depends on the field strength, history of gradient activity and heating of metallic components of the scanner, PLANET acquisition time, the used gradient mode, shimming, and more, which vary among different systems and over time. Even though the errors in estimated quantitative parameters caused by drift in human brain are small (1%-5%) compared with the errors caused by the presence of multiple components (about 30% underestimation), as we have shown in this study, they cannot be predicted and can potentially affect reproducibility of the results, as drift effects are generally not reproducible. We have now shown that the drift-induced errors can be successfully corrected by applying the proposed drift-correction algorithm. Acquiring 2 quick low-resolution reference B_0 maps before and after the PLANET acquisition

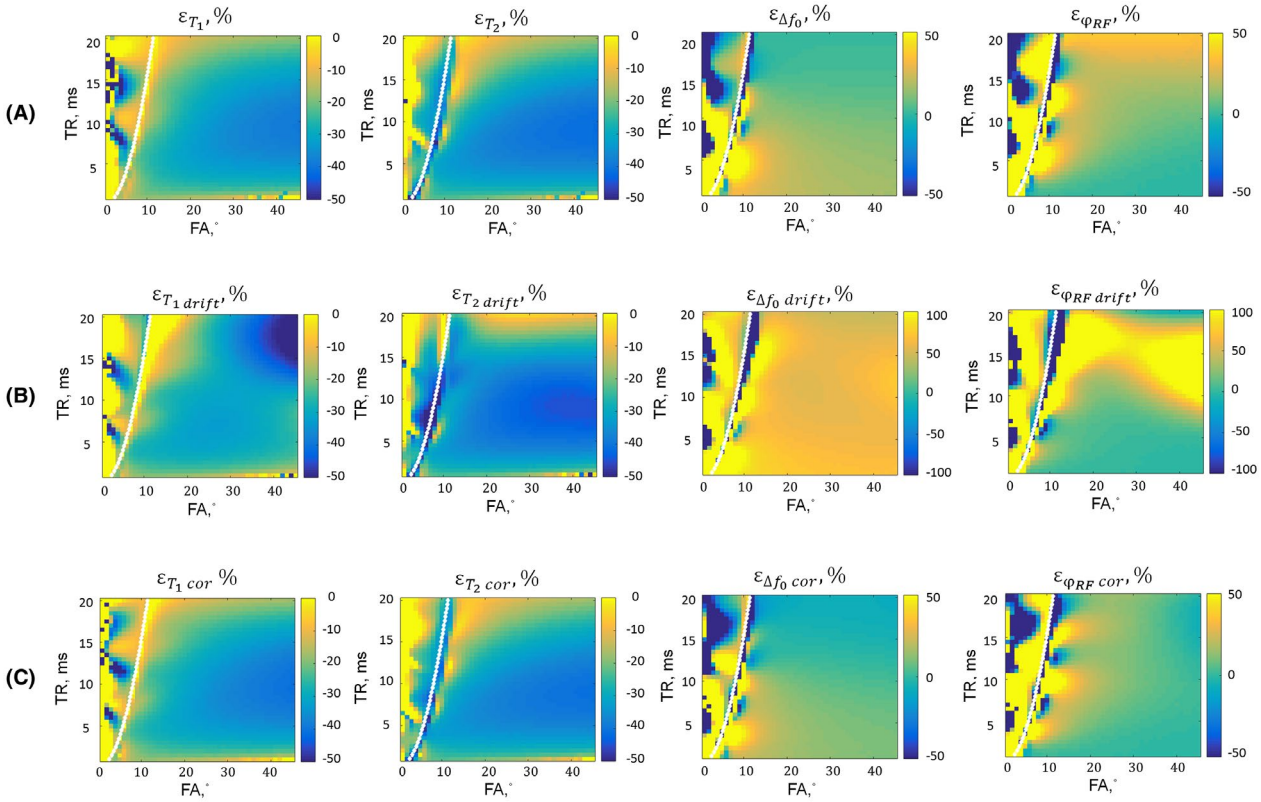

FIGURE 7 Simulation results for a two-component signal model of WM at 3 T (T_{1D} = 1000 ms, T_{2D} = 80 ms, T_{1S} = 400 ms, T_{2S} = 20 ms, Δf = 20 Hz, and myelin water fraction = 0.12). Value of Δf_0 = 10 Hz, φ_{RF} = −0.15 rad, and 10 RF phase increments. Relative errors (ε) caused by drift in T_1, T_2, Δf_0, and φ_{RF} estimates (in percent) compared with their true values (of the dominant component). A, Without drift. B, In the presence of linear over time and spatially independent drift: Δf_{drift} = [1 2 3 4 5 6 7 8 9 10] Hz. C, After linear drift-correction algorithm

is generally a simple direct way to correct for drift and improve the quantitative parameter estimation using the PLANET method.

5 | CONCLUSIONS

We have demonstrated that the PLANET method is sensitive to B_0 drift. Although there may be no directly visible B_0 drift-related artifacts on the estimated parameter maps, drift can induce errors in these parameters. In the phantom, which can be described with a single-component signal model, drift induced significant errors in the estimated parameters. However, in the human brain, where multiple components are present, drift had only a minor effect. We have now shown that the drift-induced errors can be successfully corrected by applying the proposed drift-correction algorithm for both cases of a single-component and two-component signal model.

ORCID

Yulia Shcherbakova https://orcid.org/0000-0003-3521-1767

REFERENCES

1. Cheng HL, Stikov N, Ghugre NR, Wright GA. Practical medical applications of quantitative MR relaxometry. *J Magn Reson Imaging*. 2012;36:805–824.
2. Look DC, Locker DR. Time saving in measurement of NMR and EPR relaxation times. *Rev Sci Instrum*. 1970;41:250–251.
3. In den Kleef JJ, Cuppen JJ. RLSQ: T1, T2, and rho calculations, combining ratios and least squares. *Magn Reson Med*. 1987;5:513–524.
4. Bernstein M, King KE, Zhou XJ, Fong W. *Handbook of MRI Pulse Sequences*. Amsterdam: Elsevier; 2005.
5. Schmitt P, Griswold MA, Jakob PM, et al. Inversion recovery TrueFISP: quantification of T(1), T(2), and spin density. *Magn Reson Med*. 2004;51:661–667.
6. Ehses P, Seiberlich N, Ma D, et al. IR TrueFISP with a golden-ratio-based radial readout: fast quantification of T1, T2, and proton density. *Magn Reson Med*. 2013;69:71–81.
7. Christensen KA, Grant DM, Schulman EM, Walling C. Optimal determination of relaxation times of fourier transform nuclear magnetic resonance. Determination of spin-lattice relaxation times in chemically polarized species. *J Phys Chem*. 1974;78:1971–1977.
8. Homer J, Beevers MS. Driven-equilibrium single-pulse observation of T1 relaxation. A reevaluation of a rapid "new" method for determining NMR spin-lattice relaxation times. *J Magn Reson*. 1985;63:287–297.

9. Deoni S, Rutt BK, Peters TM. Rapid combined T1 and T2 mapping using gradient recalled acquisition in the steady state. *Magn Reson Med*. 2003;49:515–526.
10. Heule R, Ganter C, Bieri O. Triple echo steady-state (TESS) relaxometry. *Magn Reson Med*. 2014;71:230–237.
11. Ma D, Gulani V, Seiberlich N, et al. Magnetic resonance fingerprinting. *Nature*. 2013;495:187–192.
12. Shcherbakova Y, van den Berg C, Moonen C, Bartels LW. PLANET: an ellipse fitting approach for simultaneous T1 and T2 mapping using phase-cycled balanced steady-state free precession. *Magn Reson Med*. 2018;79:711–722.
13. Shcherbakova Y, van den Berg C, Moonen C, Bartels LW. On the accuracy and precision of PLANET for multiparametric MRI using phase-cycled bSSFP imaging. *Magn Reson Med*. 2019;81:1534–1552.
14. Xiang QS, Hoff MN. Banding artifact removal for bSSFP imaging with an elliptical signal model. *Magn Reson Med*. 2014;71:927–933.
15. Louis LM, Frayne R. Analytical characterization of RF phase-cycled balanced steady-state free precession. *Concepts Magn Reson A*. 2009;34A:133–143.
16. Yarnykh VL. Actual flip-angle imaging in the pulsed steady state: a method for rapid three-dimensional mapping of the transmitted radiofrequency field. *Magn Reson Med*. 2007;57:192–200.
17. Bieri O, Scheffler K. Optimized balanced steady-state free precession magnetization transfer imaging. *Magn Reson Med*. 2007;58:511–518.
18. Kellner E, Dhital B, Kiselev VG, Reisert M. Gibbs-ringing artifact removal based on local subvoxel-shifts. *Magn Reson Med*. 2016;76:1574–1581.
19. Miller KL. Asymmetries of the balanced SSFP profile. Part I: Theory and observation. *Magn Reson Med*. 2010;63:385–395.
20. Miller KL, Smith SM, Jezzard P. Asymmetries of the balanced SSFP profile. Part II: White matter. *Magn Reson Med*. 2010;63:396–406.
21. Warntjes J, Dahlqvist Leinhard O, West J, Lundberg P. Rapid magnetic resonance quantification on the brain: optimization for clinical usage. *Magn Reson Med*. 2008;60:320–329.
22. Bouhrara M, Spencer RG. Rapid simultaneous high-resolution mapping of myelin water fraction and relaxation times in human brain using BMC-mcDESPOT. *NeuroImage*. 2017;147:800–811.
23. Stanisz GJ, Odrobina EE, Pun J, et al. T1, T2 relaxation and magnetization transfer in tissue at 3T. *Magn Reson Med*. 2005;54:507–512.
24. Jiang Y, Ma D, Seiberlich N, Gulani V, Griswold MA. MR fingerprinting using fast imaging with steady state precession (FISP) with spiral readout. *Magn Reson Med*. 2015;74:1621–1631.

SUPPORTING INFORMATION

Additional supporting information may be found online in the Supporting Information section at the end of the article.

TABLE S1 Quantitative results from the phantom experiment (the reference, estimated, and drift-corrected T_1, T_2, and Δf_0 values) and the relative errors in estimated and drift-corrected T_1, T_2, and Δf_0 values

How to cite this article: Shcherbakova Y, van den Berg CAT, Moonen CTW, Bartels LW. Investigation of the influence of B_0 drift on the performance of the PLANET method and an algorithm for drift correction. *Magn Reson Med*. 2019;82:1725–1740. https://doi.org/10.1002/mrm.27860